BRNO UNIVERSITY OF TECHNOLOGY

VYSOKÉ UČENÍ TECHNICKÉ V BRNĚ

FACULTY OF MECHANICAL ENGINEERING

FAKULTA STROJNÍHO INŽENÝRSTVÍ

INSTITUTE OF AUTOMOTIVE ENGINEERING

ÚSTAV AUTOMOBILNÍHO A DOPRAVNÍHO INŽENÝRSTVÍ

FLOW AND HEAT TRANSFER BETWEEN THE REAR SIDE OF A TURBOCHARGER TURBINE WHEEL AND THE BEARING HOUSING

PROUDĚNÍ A PŘENOS TEPLA MEZI ZADNÍ STRANOU TURBÍNOVÉHO KOLA TURBODMYCHADLA A LOŽISKOVOU SKŘÍNÍ

BACHELOR'S THESIS

BAKALÁŘSKÁ PRÁCE

AUTHOR — MARINA KALUGINA

AUTOR PRÁCE

SUPERVISOR — Ing. JIŘÍ VACULA

VEDOUCÍ PRÁCE

BRNO 2024

BRNO UNIVERSITY OF TECHNOLOGY
FACULTY OF MECHANICAL ENGINEERING

Assignment Bachelor's Thesis

Institut:	Institute of Automotive Engineering
Student:	**Marina Kalugina**
Degree programm:	Fundamentals of Mechanical Engineering
Branch:	Fundamentals of Mechanical Engineering
Supervisor:	**Ing. Jiří Vacula**
Academic year:	2023/24

As provided for by the Act No. 111/98 Coll. on higher education institutions and the BUT Study and Examination Regulations, the director of the Institute hereby assigns the following topic of Bachelor's Thesis:

Flow and heat transfer between the rear side of a turbocharger turbine wheel and the bearing housing

Brief Description:

Heat transfer in turbochargers is still an under–described issue. The space between the back of the turbine wheel and the bearing housing is one of the places where the heat transfer conditions are complex. Heat transfer occurs here due to radiation from the turbine wheel, convection between the rotating surface of the wheel, the gas and the stator section. The essence of this work is to analyze the heat balance at this place and apply the obtained knowledge to a real turbocharger.

Bachelor's Thesis goals:

A review of methods describing the determination of the heat balance at the point between the back of the turbine wheel and the bearing housing.
Application of the methods obtained from the research to the turbine wheel of a turbocharger.

Recommended bibliography:

CHILDS, PETER R.N. Rotating Flow. 1. Oxford: Elsevier, 2011. ISBN 978-0-12-382098-3.

BERGMAN, T. L., D. P. DEWITT, F. P. INCROPERA a A. S. LAVINE. Fundamentals of heat and mass transfer. 7th ed. Hoboken, NJ: Wiley, c2011. ISBN 978-047-0501-979.

BOYCE, M. Gas turbine Engineering Handbook, third edition, 2006, ISBN 13: 978-0-7506-7846-9.

NGUYEN-SCHÄFER, H. Rotordynamics of Automotive Turbochargers. Second Edition. Ludwigsburg, Germany: Springer, 2015. ISBN 978-3-319-17643-7.

Deadline for submission Bachelor's Thesis is given by the Schedule of the Academic year 2023/24

In Brno,

L. S.

prof. Ing. Josef Štětina, Ph.D. Director of the Institute	doc. Ing. Jiří Hlinka, Ph.D. FME dean

Abstract

The objective of the bachelor's thesis is to determine the heat balance at the point between the back of the turbine wheel and the bearing housing. The findings concerning the fluid flow and heat transfer in small channels of a rotor-stator system were derived from previously published works. The main focus of this study is the heat exchange between the heated air and the rotor wall. Calculations are applied to the turbine wheel of a real turbocharger to investigate convective heat flow at different local radii. Furthermore, a thermal resistance system is implemented in the stator section to explore potential methods for improving heat dissipation.

Abstrakt

Cílem bakalářské práce je stanovit tepelnou bilanci v místě mezi zadní stěnou turbínového kola a ložiskovou skříní. Poznatky týkající se proudění kapaliny a přenosu tepla v malých kanálech v rotor-stator systému byly odvozeny z dříve publikovaných prací. Tato studie se zaměřuje především na výměnu tepla mezi ohřátým vzduchem a stěnou rotoru. Výpočty jsou aplikovány na turbínové kolo reálného turbodmychadla ke zjištění konvektivního tepelného toku v místech o různých poloměrech. Dále je ve statorové části implementován systém tepelného odporu k prozkoumání možných způsobů pro zlepšení odvodu tepla.

Keywords
Rotating disc, fluid flow, rotor-stator cavity, friction loss, heat transfer.

Klíčová slova
Rotující disk, proudění kapaliny, rotor-stator prostor, ztráty třením, přenos tepla.

Rozšířený abstrakt

Turbínové kolo turbodmychadla musí odolávat vysokým teplotám a silnému mechanickému namáhání a je proto zvláště kritickou součástí.

Studium proudění kapalin a přenosu tepla v dutinách rotor-stator systému je předmětem intenzivního výzkumu již od velmi rané fáze.

Důležitou roli v tomto případě hraje aerodynamické chování vzduchu v kanálu. Autory provedený teoretický rozbor v rotor-stator systému společně s reálnými experimenty daly vzniknout vzorcům, ze kterých vyplívá, že výsledný točivý moment turbínového kola podléhá třecím ztrátám, jejichž velikost závisí na různých parametrech, jako je rychlost otáčení, poměr mezi velikostí axiální mezery a průměru kola, ale i například na kvalitě povrchu kola. Na velikosti točivého momentu přímo závisí teplotní energie.

Cílem bakalářské práce je analyzovat teplotní bilance v místě mezi zadní stěnou turbínového kola a ložiskovou skříní. Tepelná energie je zde přenášena prostřednictvím kondukce, konvekce a radiace. Poznatky ohledně generování a přenosu tepla v malých kanálech v rotor-stator systému jsou odvozeny z předem dostupných prací. Závěry těchto studií jsou v této bakalářské práci aplikovány na reálné turbodmychadlo.

Koeficienty tření byly vypočteny pro místa s různými průměry rotoru pro demonstrování perspektivní variability.

Provedena teplotní analýza s použitím naměřených hodnot, konkrétně na výpočty přenosu tepla z horkého vzduchu proudícího v úzkém kanálu do stěny rotujícího disku. V tomto místě nastává nucený konvekční přenos tepla a určující je zjistit hodnotu součinitele přestupu tepla. Součinitel přestupu tepla vzniká v důsledku rozdílu teplot mezi vzduchem a přilehlou stěnou rotoru a je určen na základě bezrozměrného Nusseltova čísla. Nusseltovo číslo je určeno z experimentálních výsledků pro laminární a turbulentní proudění. Výběr vzorce pro výpočet Nusseltova čísla závisí na obecných faktorech jako je rychlost, teplota, rozměr a geometrie a liší se podle konkrétní situace a cílových objektů, kdy v tomto případě jde o vzduch proudící v úzkém kanálu a přilehlý rotor.

V práci jsou pro zjednodušení hodnoty teplot proudícího vzduchu na turbínové straně zvoleny analogicky s teplotními poměry na straně kompresoru. Dále se výpočty ukazuje, že velikost tepla předaného konvekcí je přímo závislé na průměru disku a od něj se odvíjející velikosti plochy v místě výpočtu a proto je plocha disku rozdělena do čtyř segmentů a výsledná teplota je vypočítána jako jejich součet.

Rovněž byl v této práci vynechán výpočet velikosti tepelné energie vyzářené z turbínového kola radiací do statorové části, který může mít určitý vliv při vyšších teplotních gradientech avšak při velikosti teplotního gradientu uvažovaného v této studii je zanedbatelný. Přesný výpočet kondukčního přenosu tepla z kola turbíny je zanedbán kvůli komplexní geometrii turbínového kola. V práci jsou dále pouze zmíněny způsoby pro určení tepelné bilance na ložiskové straně, kde se dá použít analogie s elektrickým sériovým odporem a tak zjistit teplotu stěny ložiskové skříně. Výpočetní model statorové části je založen na

systému tří navzájem propojených rovnic.

Na závěr lze ze získaných hodnot odvodit následující: dostatečně malá drsnost povrchu disku dokáže snížit tření a tím i produkci odpadního tepla, což se projeví v efektivnějším chodu celého systému. K redukci třecího koeficientu je rovněž nutné zajistit aby proudění bylo turbulentní. Optimálního poměru mezi průměrem disku a velikostí axiální mezery je dosaženo v případě kdy se obě mezní vrstvy proudění, vznikající v mezeře jak na straně ložiskové skříně tak na straně rotoru, sjednotí. Zajištěním efektivnějšího přenosu tepla na statorové straně je možné předejít stavu, kdy je turbínové kolo konstantně namáháno provozem za vysokých teplot. Toho je možné docílit použitím materiálu s vysokou teplotní vodivostí při výrobě ložiskové skříně.

KALUGINA, M. *Flow and heat transfer between the rear side of a turbocharger turbine wheel and the bearing housing*. Brno: Vysoké učení technické v Brně, Faculty of Mechanical Engineering, 2024. 40 s. Vedoucí Ing. Jiří Vacula.

I declare that the bachelor's thesis *Flow and heat transfer between the rear side of a turbocharger turbine wheel and the bearing housing* is my own work, which I elaborated individually under Jiří Vacula's supervision. All the sources have been quoted and acknowledged by means of a complete list of references in this document.

Marina Kalugina

I would like to express my gratitude to my supervisor, Ing. Jiří Vacula, for his invaluable collaboration and guidance in helping me to achieve the objectives of my bachelor's thesis. Furthermore, I would like to thank my colleague, Ing. Jiří Klíma, for providing me with essential professional information and literature.

Marina Kalugina

Table of contents

1. Introduction

The history of the turbochargers reveals a close relationship with the automotive industry. In 1885, Gottlieb Daimler and Rudolf Diesel initiated research into enhancing power output and reducing fuel consumption by compressing the air injected into the combustion chamber. This concept subsequently gave rise to the development of turbochargers. Nevertheless, the breakthrough was achieved by Alfred Büchi. In 1925, he became the first to effectively implement supercharging using exhaust gases, thereby achieving an increase in power of 40%.

Over time, the fundamental principles underlying the operation of turbochargers have remained consistent. Nevertheless, there have been significant enhancements to the design. This evolution has been driven by the broadening of their applications.

During the 1930s, turbocharging was employed in large engines used in ships, locomotives and industrial engines. Subsequently, gave rise to a period of accelerated technological advancement in the field of gas turbines for aircraft. At this juncture, extensive research was conducted into new materials and designs were made, resulting in significant advancements in turbocharger technology for diesel engines. Subsequently, the development of the first compact model of turbochargers for trucks and passenger cars commenced. The initial turbocharged automobiles were not particularly successful due to their high fuel consumption, low torque and poor reliability.

The technology of exhaust gas turbocharging is now employed all over the world. This implies that the output from a given construction volume can be up to four times greater. Consequently, the same performance can be achieved with significantly less material, installation space and costs. Moreover, there has been a decline in fuel consumption and pollutant emissions, which aligns with the economic and ecological improvements.

In recent years, there has been a need to identify potential solutions to optimise the boosting technology. One such solution is the electrically driven turbocharger, which can provide additional boost at low engine speeds or generate electricity at high engine speeds. The hybrid turbocharger regulates the speed of the turbocharger by discharging a percentage of air into the ambient.

The transition from conventional internal combustion engines to alternative powertrains will result in changes to the technology and market for turbochargers. Battery electric vehicles represent a prime example, as they do not require turbochargers. The widespread deployment of these technologies would considerably reduce the size of the turbocharger market. Nevertheless, it is unlikely that this transition will entirely supplant conventional turbochargers. The necessity for high turbocharger efficiency, durability and low manufacturing cost will remain.

2. Turbocharger components

Nguyen-Schäfer [1] noted that automotive turbochargers are applied the intense heat produced by exhaust gases, reaching around 820–850 °C in diesel engines and 950–1050 °C in gasoline engines. High exhaust gas temperatures transfer a significant amount of heat into the turbine wheel. Consequently, a portion of this heat tends to travel into the bearing housing and shaft of the turbocharger, as these components have lower temperatures. This chapter provides an overview of the turbocharger components exposed to high heat as a consequence of exhaust gases. Additionally, the cooling systems within the bearing casing are described in further detail.

2.1. The radial flow turbine

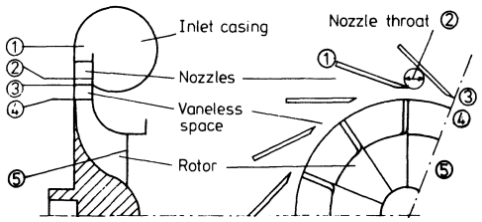

Figure 2.1: Radial flow turbine, adopted from [2]

The turbine with radial inflow is the first choice for high-speed turbochargers. This configuration allows for high efficiency due to the achievement of a high expansion ratio. Figure 2.1 represents a cross-sectional view of the radial flow turbine and the approximate interaction of the nozzle vanes with turbine blades.

Watson and Janota [2] delineated the principal functions of the turbocharger turbine, wherein the construction of the turbine side is analogous to that of the compressor side, with the exception of the reversed fluid flow function.

- *Turbine inlet casing or volute* is connected to the engine's exhaust manifold by a sealed flange. The volute casing is designed to ensure a consistent fluid flow, with the optimal shape facilitating this. Subsequently, the exhaust gases are directed radially from the inlet casing to the nozzle vanes.

- *Nozzle ring* reduces the pressure energy of expanded gases, converting it to the kinetic energy and thereby accelerating the flow. It is composed of blades that can be installed at different angles for optimal maching of the turbocharger to the engine. The objective is to achieve an effective fluid transfer to the turbine wheel with minimal losses.

- *Turbine wheel* takes over the kinetic energy onto the turbine blades and converts it into mechanical power to drive the rotor shaft. As a result, the kinetic energy of the exhaust gases is reduced. The remaining exhaust gases contain a residual quantity of pressure and thermal energy [1].

- *Turbine outlet casing* serves to discharge exhaust gases, which are propelled in an axial direction by the impeller. Furthermore, the turbine outlet casing facilitates the dissipation of heat generated by the high-temperature gases.

2.1.1. Aerothermodynamics

Isentropic efficiency

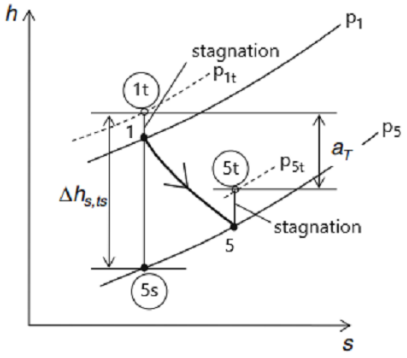

Figure 2.2: Turbine stage expansion in *h-s* diagram, edited and adopted from [1]

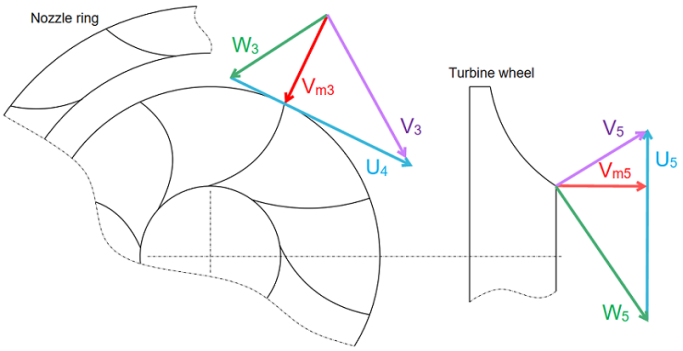

Figure 2.3: Velocity vectors in radial turbine flow

The enthalpy diagram in figure 2.2 illustrates the isentropic and polytropic expansion of exhaust gases from the turbine inlet to the turbine outlet casing. The turbine efficiency η_T [-] can be calculated as the ratio of ideal to actual work:

$$\eta_T = \frac{h_{1t} - h_{5t}}{h_{1t} - h_{5s}} \tag{2.1}$$

where h_{5s} [J kg^{-1}] is the specific enthalpy in the turbine outlet casing without losses, h_{1t} [J kg^{-1}] is the specific enthalpy in the inlet casing and h_{5t} [J kg^{-1}] in the outlet casing, respectively.

Velocity triangles

Watson and Janota [2] described the derivation of energy transfer using velocity triangles. Figure 2.3 depicts the velocity vectors entering and leaving the impeller. The absolute fluid velocity V_3 [m s^{-1}] and its radial vector V_{m3} [m s^{-1}] lead the rotor while the fluid velocity relative to the rotor blades is W_3 [m s^{-1}]. From this, the rotor tip speed is U_4 [m s^{-1}]. At the rotor outflow, the absolute fluid velocity is V_5 [m s^{-1}] and its axial vector V_{m5} [m s^{-1}], respectively. Due to the blade speed U_5 [m s^{-1}], the relative fluid velocity will be W_5 [m s^{-1}].

Euler turbine equation

Watson and Janota [2] observed that the stagnation enthalpy h_{1t} [J kg^{-1}] at the gas admission casing is equivalent to the enthalpy at the rotor since no work is done in the volute and nozzle ring. The Euler turbine equation for the rotor can be defined as

$$h_{5t} - h_{1t} = \frac{1}{2} \cdot \left[(V_3^2 - V_5^2) + (U_4^2 - U_5^2) + (W_5^2 - W_3^2) \right] \tag{2.2}$$

The total turbine energy transfer $\dot{W}$ [W], respectively

$$\dot{W} = (h_{5t} - h_{1t}) \cdot \dot{m}_T \tag{2.3}$$

where $\dot{m}_T$ [kg s^{-1}] is mass flow rate.
The effective turbine output power P_T [W] is

$$P_T = \eta_T \cdot \dot{m}_T \cdot c_p \cdot T_1 \cdot \left[1 - \left(\frac{p_5}{p_1} \right)^{\left(\frac{\kappa - 1}{\kappa} \right)} \right] \tag{2.4}$$

where c_p [J kg^{-1} K^{-1}] is the specific heat capacity at constant pressure; T_1 [K] and p_1 [Pa] are the temperature and pressure in the inlet casing; p_5 [Pa] is the pressure in the turbine outlet casing, $\kappa \approx 1{,}4$ [-] is the isentropic exponent of the air.

2.2. Turbocharger rotor and bearing system

Nguyen-Schäfer [1] mentioned that the bearing system plays a crucial role in supporting the rotor during operation. The thrust and radial bearings help maintain the proper alignment and allow the rotor to rotate smoothly within the housing. Furthermore, the bearing system ensures the transfer of axial and radial loads generated by the rotating components. This is essential for ensuring the turbocharger's reliability, longevity, and overall performance. Efficient lubrication and proper cooling of the bearings are also key factors in managing the heat generated during operation and maintaining optimal operating conditions.

Figure 2.4 illustrates design of the bearing system that includes bearings, the rotor shaft, turbine and compressor wheels. The sleeve or bearing casing provides structural support and contains the rotating shaft assembly within the turbocharger. Additionally, it contains the lubricating oil passages and seals. The thrust bearing is situated between the thrust rings and securely positioned within the bearing housing. The force on the thrust bearing arises from the compression of the oil film situated between the bearing and thrust rings. Therefore, the thickness of the oil film determines the reactive force of the thrust bearing. It is important to note that a smaller oil film thickness results in a larger thrust bearing force, and conversely, a larger oil film thickness leads to a smaller thrust bearing force. [1] There are two main types of radial bearings commonly used in turbochargers:

Hydrodynamic bearing system

Hydrodynamic fluid film bearings gain an advantage at higher rotor speeds due to their operation based on the principle of hydrodynamic lubrication. The fluid not only lubricates the parts, preventing contact, but also controls the motion of the shaft and wheels

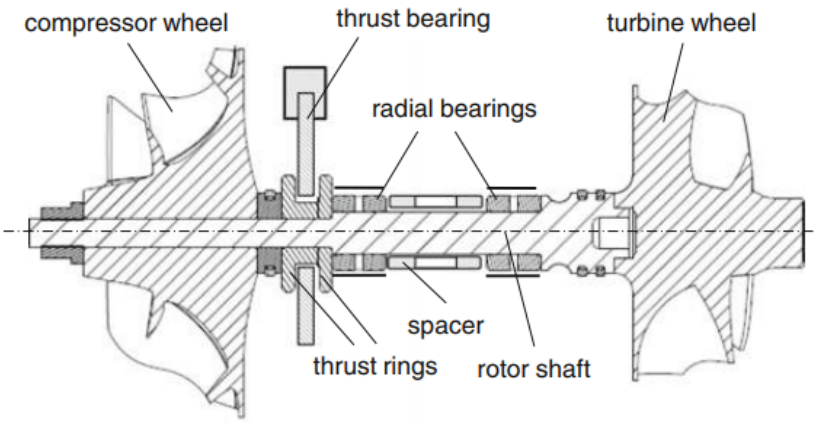

Figure 2.4: Rotor and bearing system in a turbocharger, adopted from [1]

under all running conditions. The hydrodynamic bearing system uses two fully floating journal bearings, which rotate at approximately half the speed of the shaft. There are two hydrodynamic oil films: an outer one and an inner between the bearing and the shaft. High speed passenger vehicle turbochargers use a one piece semi-floating bearing which does not rotate. This design also uses two oil films, but in this case the outer oil film acts mainly for damping shaft motion. On this bearing, there is only one hydrodynamic oil film between the shaft and the bearing. [3]

Ball bearing system

Ball bearings offer reduced friction, which means faster response times and increased durability. Reduced clearances enhance turbine and compressor performance, lowering power losses within the bearing and improving overall efficiency. [3]

2.2.1. Rotor shaft

The rotor conducts a significant quantity of heat from the turbine to the internal lubrication layer. Then a considerable amount of heat is consistently transferred from the inner layer to the outer layer through the sleeve. In the journal bearing on the turbine side, the heat is drawn away from the rotor by the lubricant flow and is subsequently expelled from the system through convective heat exchange. [4]
Several factors increase the temperature of the rotor, which are:

- High rotary speed: Operation at high speeds can lead to increased friction and heat generation within the rotor.
- Increased boost pressure: Higher boost pressure, aimed at improving turbocharger efficiency, affects the temperature of the rotor.
- Insufficient lubrication: Poor lubrication results in increased friction and heat generation.
- Exhaust gases: The rotor contributes to extremely high exhaust gas temperatures, resulting in elevated overall temperatures.

- Restricted airflow: Inadequate design results in insufficient ventilation.
- Oil contamination
- Rotor vibrations: Mechanical and thermal imbalances lead to the generation of stresses and an increase in rotor temperatures.
- Mechanical deformations: Deformed components within the assembly modify the clearance width, leading to forced flow and increased temperatures.

2.3. Lubrication oil system

The role of lubrication is to reduce dissipating heat and the friction between the moving parts. Goldfarb & Associates [5] clarified that once installed, the turbocharger is linked to the engine's lubrication and cooling mechanisms. Lubricating the bearings using the engine oil system is a cost-effective solution as long as the oil quality meets the required filtration standards.
Further elucidations from Goldfarb & Associates [5] indicated that the oil pump is responsible for moving lubricating oil from the oil pan to the turbocharger. Prior to reaching the turbocharger, the oil passes through an oil filter to eliminate impurities. Subsequently, an oil feed line directs the oil to the turbocharger. Within the bearing housing, the oil lubricates the bearings and the rotating shaft. After passing through the bearing housing, the oil returns to the oil pan through an oil return line. This cycle repeats constantly while the engine is in operation. The consistent oil flow is ensured to maintain the smooth operation of the turbocharger.
Nguyen-Schäfer [1] observed that the operational oil temperature within the bearing casing typically ranges 30–50 °C higher than the inlet temperature and remains below the oil coking temperature. However, reducing the oil inlet temperature at some point leads to an increase in bearing friction power.

2.4. Water-cooled system

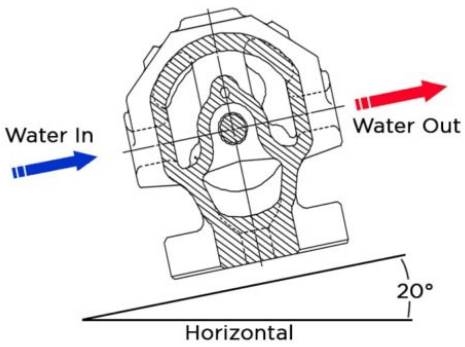

Figure 2.5: Cross section view of water-cooled bearing casing, adopted from [6]

Garrett [6] provided data indicating that the majority of the heat is absorbed by the oil while the engine is in operation and the oil is circulating through the bearing system.

Furthermore, it is possible for some turbochargers to be cooled by water. The coolant is a mixture of water and antifreeze. Water cooling ports are located on both sides of the bearing housing. Heat within the bearing casing is transferred to the water. As the water flows through the turbocharger and absorbs heat, it naturally rises through the cooling system, protecting bearings and seals against damage from excessive heat. To achieve optimal cooling efficiency, the bearing casing must be installed at a horizontal angle of 20 °. The water line setup of the water-cooled Garrett bearing casing is shown in figure 2.5. Input water is directed into the lower port, while the hotter output water is pumped from the higher port further into the engine's cooling system. This configuration promotes efficient thermal siphoning after the engine is shut down.

3. Flow in rotor-stator cavity

The primary rotor losses that impact the efficiency of the turbocharger include fluid friction within the passages, disc friction on the wheel and clearance effects [2]. Disc friction losses occur between the rear side of the turbine wheel and the wall of the bearing casing. Fluid flow in the axial clearance causes a power loss. Experimental results indicate that friction loss is influenced by the axial gap, Reynolds number and surface roughness. This chapter provides an overview of a rotating disc, offering insights into the intricacies of fluid dynamics applicable to both laminar and turbulent flows.

3.1. General flow theory

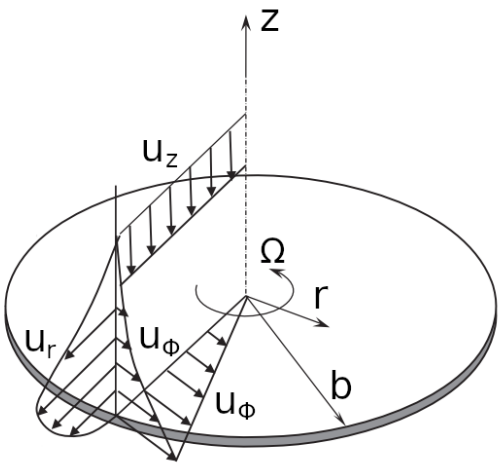

Figure 3.1: Flow distribution on the free rotating disc, edited and adopted from [7]

To better understand the flow theory, the free disc rotating in a stationary fluid is considered. Radial, tangential and axial velocity distributions are illustrated in figure 3.1. The disc of outer radius $b\,[\mathrm{m}]$ rotates with an angular velocity $\Omega\,[\mathrm{rad\ s^{-1}}]$ about the z-axis $[\mathrm{m}]$. The tangential velocity $u_\phi\,[\mathrm{m\ s^{-1}}]$ of the fluid is sheared from the disc speed. The radial velocity $u_r\,[\mathrm{m\ s^{-1}}]$ is distributed in the boundary layer of the disc. The radial and tangential velocity components increase linearly with the local radius $r\,[\mathrm{m}]$. At the central axis of the disc, both the radial and tangential velocities are equal to zero. The axial flow $u_z\,[\mathrm{m\ s^{-1}}]$ is directed towards the disk. The viscous force in the radial direction is in equilibrium with the centrifugal force and rises as the radius of the disc increases. While the viscous force in the tangential direction is in equilibrium with the angular momentum of the flow, reaching its maximum at the surface of the rotating disc. [8]

3.2. Rotor-stator disc cavity

The rotating disc of the turbine wheel and the wall of the bearing casing as the stator together form a cavity known as a rotor-stator cavity or wheelspace. The gap formed between the stationary casing and the rear face of the impeller can be considered as an enclosed rotor-stator cavity if no through flow is supplied into the system [8].

3.2.1. Enclosed rotating disc

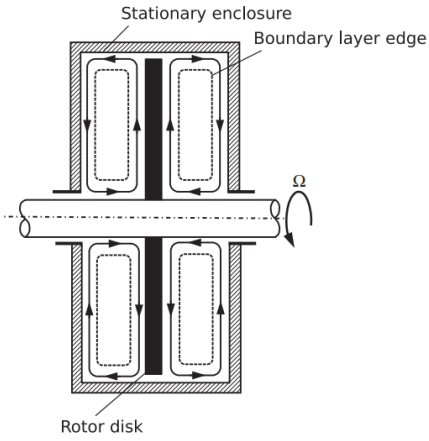

Figure 3.2: Enclosed rotor disc, adopted from [7]

The presence of a stationary shroud affects the flow pattern along the disc surface and the stationary wall. Figure 3.2 illustrates how the disc rotates within a stationary housing without inflow or outflow. Along the rotor surface, the fluid is radially expelled, folowed by axial flow from the rotor boundary layer to the stator boundary layer. Subsequently, the fluid is pumped along the stator radially inwards and returned axially to the rotating disc. [7]

3.2.2. Classification of flow regimes

Daily and Nece [9] performed experimental and theoretical verification of flow regimes between the rotating disc and the stationary wall without superposed flow. The investigation was obtained for the range of disc Reynolds numbers Re_ϕ [-] from 1×10^3 to 1×10^7. Axial clearance s [m] between the rotor and the stator were varied ratios s/b [-] from 0,0127 to 0,217. These regimes are:

- Regime I: Laminar flow with merged boundary layers.
  Boundary layers on the rotor and stator are merged. Laminar flow with lower Reynolds numbers.

- Regime II: Laminar flow with separate boundary layers.
  The sum of the boundary layers on the rotor and stator is less than the axial gap. Laminar flow with lower Reynolds numbers.

- Regime III: Turbulent flow with merged boundary layers.
  Boundary layers on the rotor and stator are merged. Turbulent flow with higher Reynolds numbers.

- Regime IV: Turbulent flow with separate boundary layers.
  The sum of the boundary layers on the rotor and stator is less than the axial gap. Turbulent flow with higher Reynolds numbers.

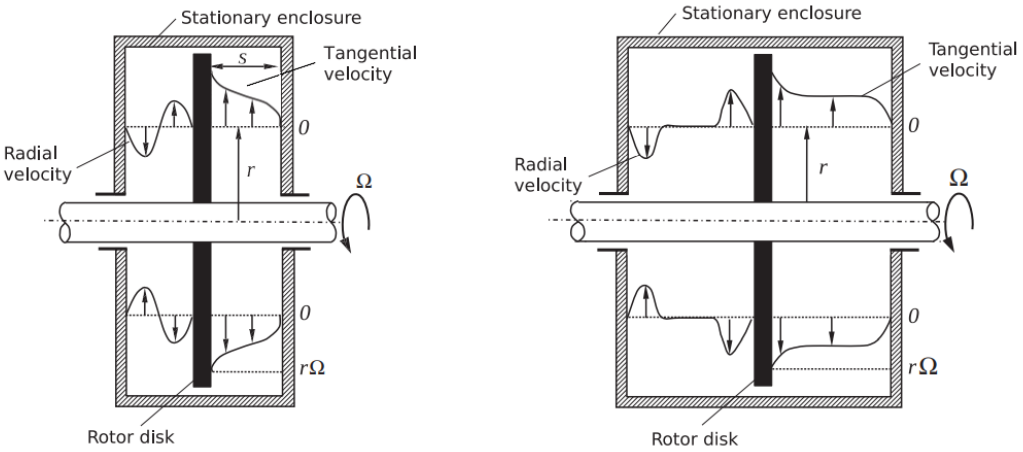

(a) Regime III, merged boundary layers (b) Regime IV, separate boundary layers

Figure 3.3: Velocity profiles in enclosed rotor-stator system, edited and adopted from [7]

Figures 3.3a and 3.3b represent velocity profiles for the radial and tangential components in an enclosed rotor-stator system for regimes III and IV, which are more likely to occur in the wheelspace between turbine disc and bearing casing wall under operating conditions. Childs [8] noted the existence of an inviscid core of fluid between boundary layers on the rotor and stator. The core of fluid rotates as a solid body with some fraction of the rotor angular velocity. The rotating core has negligible movement in the radial direction, while the tangential velocity is represented by the constant $0{,}44\Omega r$ [10]. Childs [8] further indicated that the Batchelor flow model is likely to occur in cavities with large axial clearance, including regimes II and IV. Regimes I and III represent Couette flow, where the flow in a narrow gap is dominated by viscous forces. Daily and Nece [9] established correlations for the moment coefficient c_m [-] for one face of the disc for each flow model. The ratio s/b can be simplified as the dimensionless gap width G [-]:

$$G = \frac{s}{b} \tag{3.1}$$

Regime I is expressed as

$$c_m = \frac{\pi}{G \cdot Re_\phi} \tag{3.2}$$

Regime II is expressed as

$$c_m = 1{,}85 \cdot G^{\frac{1}{10}} \cdot Re_\phi^{-\frac{1}{2}} \tag{3.3}$$

Regime III is expressed as

$$c_m = 0{,}04 \cdot G^{-\frac{1}{6}} \cdot Re_\phi^{-\frac{1}{4}} \tag{3.4}$$

Regime IV is expressed as

$$c_m = 0{,}0051 \cdot G^{\frac{1}{10}} \cdot Re_\phi^{-\frac{1}{5}} \tag{3.5}$$

The flow rate coefficient c_w [-] is defined as

$$c_w = \frac{\dot{m}}{\mu \cdot b} \tag{3.6}$$

where $\dot{m}$ [kg s^{-1}] is mass flow rate in the cavity and μ [Pa s] is the fluid dynamic viscosity. $c_w = 0$ indicates an enclosed wheelspace with no superimposed throughflow [10].

3.3. The disk friction loss calculation

Aerodynamic power dissipation can be determined by utilizing empirical correlations that consider the geometrical parameters of the rotor-stator system, its rotational speed, and the density of the working fluid.
Childs [8] put forth the following calculation in the case of large axial clearances.
The angular velocity of the disc is given by

$$\Omega = \frac{2 \cdot \pi \cdot n}{60} \tag{3.7}$$

where n [rpm] is the rotational speed.
The rotational Reynolds number can be determined by

$$Re_\phi = \frac{\Omega \cdot b^2 \cdot \rho}{\mu} = \frac{\Omega \cdot b^2}{\nu} \tag{3.8}$$

where ρ [kg m^{-3}] is the fluid density and ν [m^2 s^{-1}] is the kinematic viscosity of the working fluid.
The flow is considered laminar if the rotational Reynolds number is lower than 2×10^5. Otherwise, the flow is turbulent. However, in real cases where the axial wheelspace is much smaller, the distinction between laminar and turbulent flow is dependent not only on the values of Re_ϕ but also on the axial gap width.
The boundary layer thickness δ [m] for laminar flow over a single disc is dependent on viscosity, and along the entire layer, it remains constant, equation 3.9. Meanwhile, for turbulent flow, the thickness of the boundary layer increases with the local radius, equation 3.10.

$$\delta = 5{,}5 \cdot \sqrt{\frac{\mu}{\Omega \cdot \rho}} \tag{3.9}$$

$$\delta = r^{\frac{3}{5}} \cdot \left(\frac{\mu}{\Omega \cdot \rho} \right)^{\frac{1}{5}} \tag{3.10}$$

Knowing the results, whether the flow is laminar or turbulent, together with the result of whether the layers are merged $s \leq 2 \cdot \delta$ or separated $s > 2 \cdot \delta$, it becomes possible to identify the flow regime and select the equation for the moment coefficient. The moment on the disc face T_q [N m] is determined as follows

$$T_q = 0{,}5 \cdot \rho \cdot \Omega^2 \cdot b^5 \cdot c_m \tag{3.11}$$

Mechanical power dissipation P_{DF} [W] or the power needed to spin the disc and overcome frictional drag on its surface

$$P_{DF} = T_q \cdot \Omega \tag{3.12}$$

Transition to turbulent flow

Beretta and Malfa [11] presented equations that enable the identification of the transition to turbulent flow in enclosed rotor-stator systems. The equations are presented below, with the relevant axial wheelspace indicated.

$$Re_\phi > \left(\frac{\pi}{0{,}036}\right)^{\frac{4}{3}} \cdot G^{-\frac{10}{9}}, \quad G < 0{,}0111 \tag{3.13}$$

$$Re_\phi > \left(\frac{1{,}85}{0{,}036}\right)^{4} \cdot G^{\frac{16}{15}}, \quad 0{,}0111 < G < 0{,}0233 \tag{3.14}$$

$$Re_\phi > \left(\frac{1{,}85}{0{,}0545}\right)^{\frac{10}{3}}, \quad G > 0{,}0233 \tag{3.15}$$

3.4. Further investigation and improvement

3.4.1. Application in air with high-speed condition

Goulburn and Wilson [12] optimized the approach to power losses in a rotating disc in high-speed turbomachinery operating in air. Experiments were conducted on the test rig and compared with the previous theory proposed by Daily and Nece. Specifications of the disc are presented in table 3.1.

Table 3.1: Rotating disc data

Parameter	Dimension
Gap ratio (G)	0,004; 0,0124 and 0,05
Disc diameter	127 mm
Disc thickness	6,35 mm
Reynolds number (Re_ϕ)	1×10^6
Working fluid	synthesis gas
Surface finish	smooth

Experimental setup

In this experiment, a test rig was powered by a turbine unit capable of reaching speeds of 66000 rpm. The rotational speed was quantified by means of a capacitance probe placed within the housing to register the passing of each turbine rotor vane. Torque was regulated by a dynamometer.

Test results

The results of the torque coefficient were compared with the previous theory, where the cavity contained liquid flow and the rotational speed was thirty times lower. It showed good agreement for small axial clearances at high Reynolds numbers. However, the correlation was not strong for the ratio of 0,05. Recommendations were made that the theory may be applied to compressible (air) and incompressible (liquid) fluids across a wide range

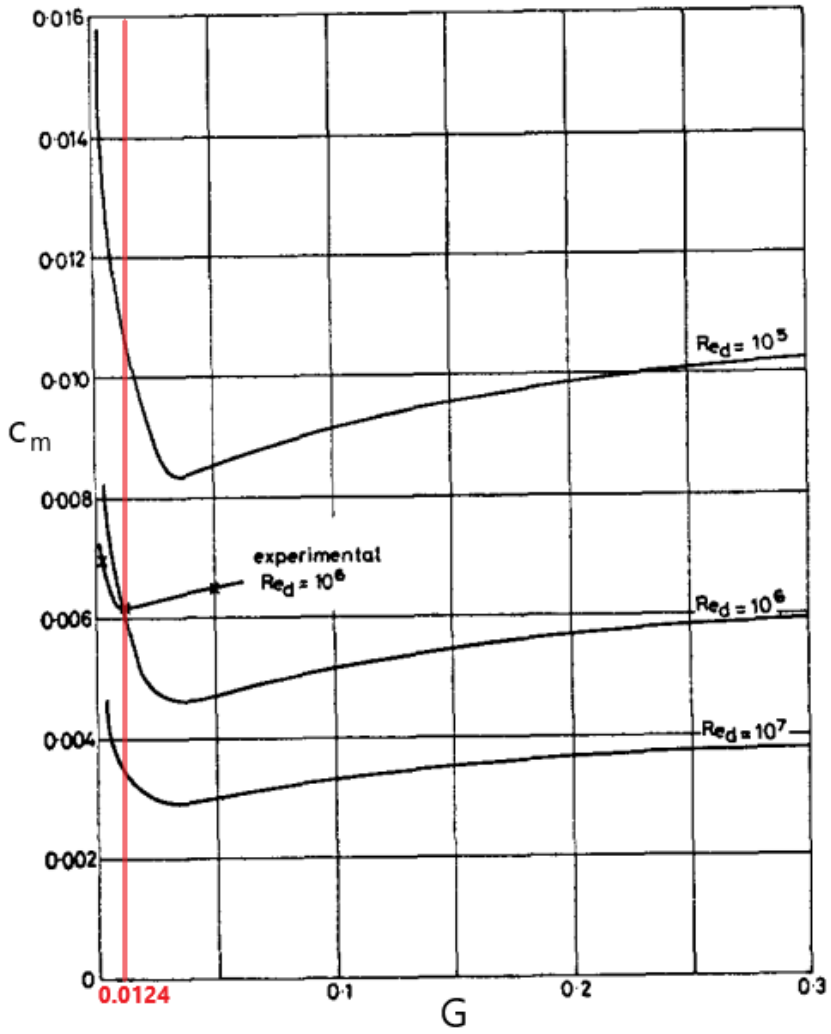

Figure 3.4: Relationship between moment coefficient and gap ratio, edited and adopted from [12]

of speeds and sizes when dealing with small clearance ratios (under 0,0124). [12]
Figure 3.4 illustrates the correlation between the moment coefficient and axial clearance ratio, comparing the Daily and Nece theory with experimental data. Based on experimental data, the minimum moment coefficient occurs at a ratio of 0,0124, indicating the optimal axial clearance for minimizing losses. [12]

3.4.2. Influence of surface roughness

Poullikkas [13] introduced the impact of surface roughness by examining the enclosed rotating disc with turbulent flow and separate boundary layers. Specifications of the disc are presented in table 3.2. Subsequently, a new empirical equation for the disc friction coefficient involving the surface roughness parameter k_a [m] is provided below:

$$c_m = \left(\frac{k_a}{b}\right)^{\frac{1}{4}} \cdot G^{\frac{1}{10}} \cdot Re_\phi^{-\frac{1}{5}} \tag{3.16}$$

Table 3.2: Rotating disc data

Parameter	Dimension
Gap ratio (G)	from 0,0333 to 0,1267
Tip ratio (t/b)	0,1467
Reynolds number (Re_ϕ)	$3{,}83 \times 10^6$
Working fluid	water
Surface roughness (k_a)	0,0261; 0,0163 and 0,0083 mm

Experimental setup

In this experiment, a test platform equipped with a motor capable of reaching speeds of up to 2000 rpm was used. Torque was determined using foil strain gauges, the water temperature was measured using thermocouples, and the flow rate was monitored using variable area flowmeters.

Test results

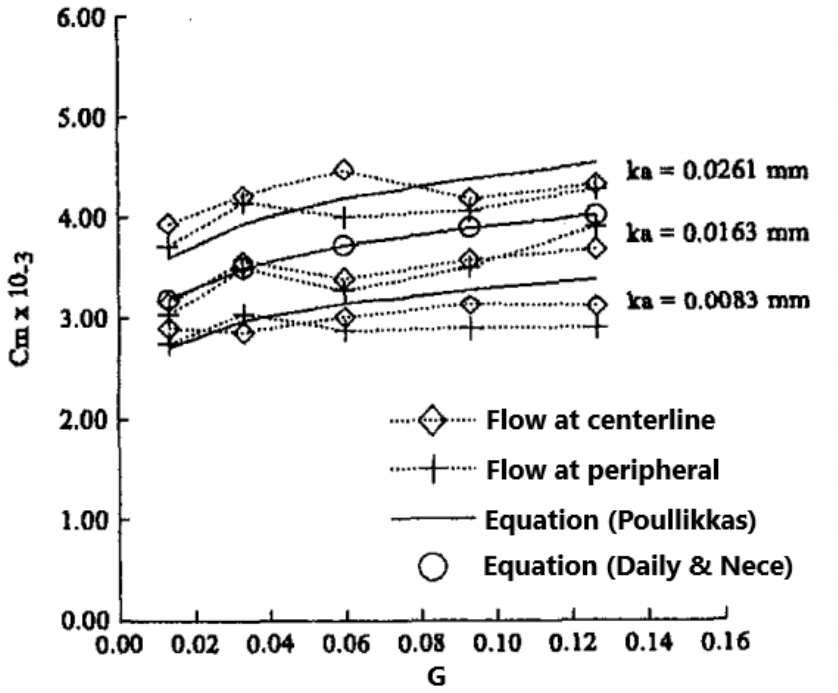

Figure 3.5: Comparison of experimental results and empirical equations, edited and adopted from [13]

Further comparison of experimental results with empirical equations is graphically shown in figure 3.5. Both experimental and theoretical findings highlight that a rough surface leads to an increase in the disc friction coefficient. Experimental leakage flow at the periphery, namely flow acting radially on the width of the disc and continuing along the outer edge, results in overall lower friction losses compared to the leakage flow at the centerline, namely flow acting axially on the disc face. The equation 3.5 proposed by Daily and Nece is valid for the surface roughness parameter of 0,0163 mm. The equation 3.16 is

applicable in practice for regime IV as it does not exceed an error of 9% when compared to experimental results. [13]

Alternative solution

Nemdili and Hellmann [14] considered a method to calculate the friction loss coefficient for both smooth and rough discs. The following equation can be used to determine the critical value for hydraulic roughness $k_{a,crit}$ [m]:

$$k_{a,crit} = \frac{150 \cdot \nu}{\Omega \cdot b} \tag{3.17}$$

For the regime with hydraulic smooth surface

$$c_m = 0{,}075 \cdot Re_\phi^{-\frac{1}{5}} \cdot \left[1 + 0{,}75 \cdot \left(G + \frac{t}{b}\right)\right], \qquad k_a \leq k_{a,crit} \tag{3.18}$$

where t [m] is the radial gap between the disc and the housing.
For the regime with hydraulic rough surface

$$c_m = \frac{1 + 0{,}75 \cdot \frac{t}{b}}{\left[3{,}8 \cdot \log_{10}\left(\frac{b}{k_a}\right) - 2{,}4 \cdot G^{\frac{1}{4}}\right]^2}, \qquad k_a \geq k_{a,crit} \tag{3.19}$$

3.4.3. Influence of scallops

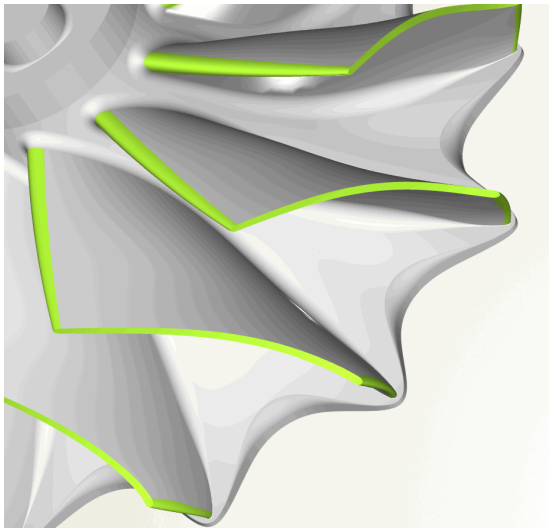

Figure 3.6: Turbine wheel scallops, edited and adopted from [15]

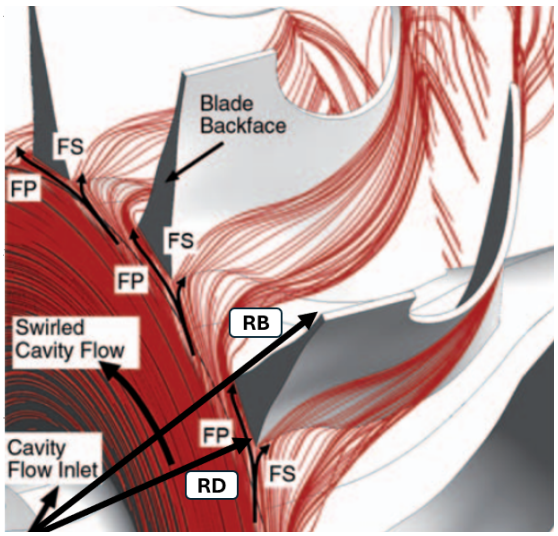

Figure 3.7: Backface cavity clearance flow, edited and adopted from [16]

The turbine wheel is subjected to significant thermal stresses during engine startups and shutdowns. One possible solution to reduce compressive and tensile loads is the use of a turbine wheel with scalloped areas. Figure 3.6 represents a turbine wheel with blades placed between scalloped arcs. Nguyen-Schäfer [1] confirmed that while the use of a scalloped turbine disc does result in a reduction in the mass of the heavy inconel turbine wheel, it also leads to a decrease in the turbine's effective power. He et al. [16] conducted an investigation into the flow of backface cavity clearance in scalloped radial turbines.

Figure 3.7 illustrates the flow structure within the rear disc cavity, which extends into the mainstream. At the outer disc radius, the clearance flow is divided into two streams FP and FS, which cover the blade and merge.
The findings of He et al. [16] indicate that the backface cavity clearance flow has a relatively low impact on scalloped turbine efficiency compared to other clearance losses. Moreover, it was established that the radius ratio RD/RB of 0,8 results in an overall high efficiency. Nevertheless, a deeply scalloped turbine of 0,6 is identified as the optimal ratio for reducing compressive and tensile loads.

3.5. Summary

An overview of an enclosed rotor-stator system with different flow regimes has been given. The objective for real-world applications is to establish a flow regime throughout the entire cavity that is characterized by merged boundary layers and turbulent fluid flow. In contrast to laminar flow, turbulent fluid flow is less dependent on viscosity, which results in a reduction in frictional losses. Near the axis of rotation, the probability of laminar flow is high due to the correlation between the circumferential Reynolds number and the local disc radius. One potential approach to maintaining turbulent flow at the inner disc radius is to reduce the axial clearance near the axis of rotation. It is also important to consider the potential for an increase in the radial velocity distribution. The investigation into the influence on flow behavior and power loss yielded significant results in relation to surface roughness and scalloped disc design.

4. Heat transfer in rotor-stator cavity

Heat transfer can be defined as the process of transporting heat from a region of higher temperature to a region of lower temperature. The rate at which heat is transferred per unit of time is denoted as the heat flow rate, represented by $\dot{Q}$ [W]. The heat flux $\dot{q}$ [W m^{-2}] is determined by the amount of heat transferred per unit of time and per unit area perpendicular to the direction of heat flow. The heat transfer can be divided into three modes:

- *Convection* refers to the exchange of energy between a surface and a fluid in motion across that surface. This process encompasses the transfer of energy through both the overall movement of the fluid and the random motion of its individual molecules.

- *Thermal radiation* is designated as the energy released by any substance into its environment through electromagnetic waves. Electromagnetic waves have the ability to travel through a vacuum.

- *Conduction* involves the transfer of energy through molecular interactions between adjacent molecules, induced by their random movement. Heat conduction can occur within solids, liquids, or gases. As the temperature rises, the random motion of molecules becomes more pronounced.

4.1. Convective heat transfer

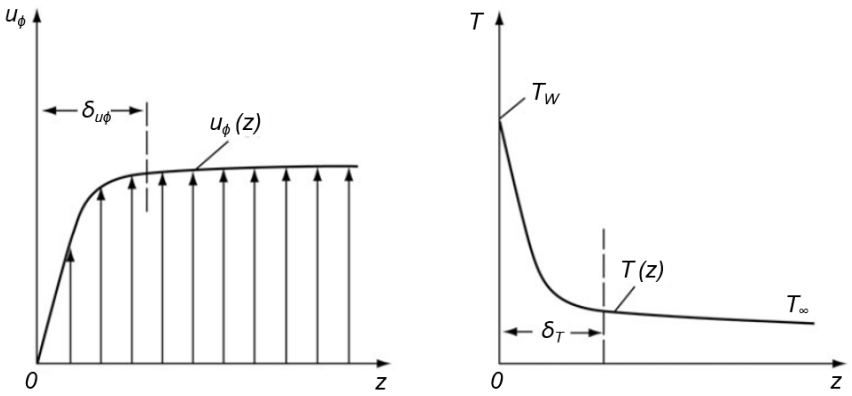

Figure 4.1: Velocity and temperature boundary layers, edited and adopted from [18]

Convective heat transfer involves two main mechanisms. Firstly, there is the transfer of energy caused by the random movement of molecules, known as diffusion. Secondly, energy is transferred through a large number of molecules in the fluid. This bulk motion of the fluid, which occurs simultaneously with random molecular motion, contributes to heat transfer. In the presence of a temperature gradient, this fluid motion enhances heat

transfer. [17]
When a fluid flows over a heated surface, it creates a specific area in the fluid where the velocity changes from zero at the surface to a finite value. This zone is known as the velocity boundary layer in figure 4.1. Additionally, if there is a temperature difference between the surface and the flowing fluid, there will be another area in the fluid where the temperature changes from the surface temperature T_W [K] to the temperature of the outer flow T_∞ [K]. This area is called the thermal boundary layer. [17]
When external forces, such as fans, pumps, or atmospheric winds, drive the flow, it is called forced convection. On the other hand, when the flow is induced by buoyancy forces caused by density differences due to temperature variations in the fluid, it is termed free or natural convection. [17]

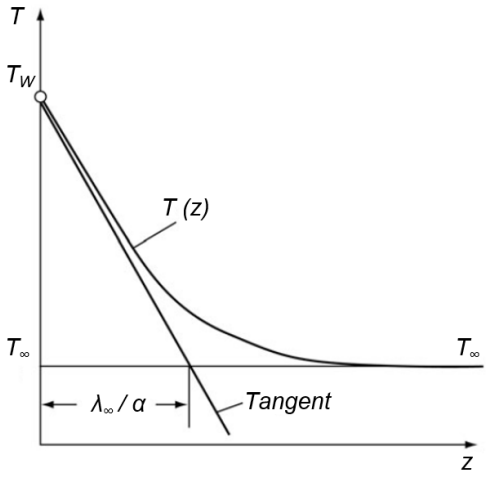

Figure 4.2: Thermal boundary layer thickness, edited and adopted from [18]

The heat flux $\dot{q_{conv}}$ is influenced by material properties, temperature difference and by the temperature and velocity distributions within the boundary layer. [17]
Convection heat transfer and Newton's law:

$$\dot{q_{conv}} = \alpha \cdot (T_W - T_\infty) \tag{4.1}$$

where α [W m^{-2} K^{-1}] is the convection heat transfer coefficient.
The convection heat transfer coefficient depends on conditions within the boundary layer. These conditions are shaped by factors like surface geometry, the type of fluid movement, and various thermodynamic and transport properties of the fluid. [17]
The VDI Heat Atlas [18] states that the thermal boundary layer thickness δ_T [m] depicted in figure 4.2 can be approximated by

$$\delta_T \approx \frac{\lambda_\infty}{\alpha} \tag{4.2}$$

where λ_∞ [W m^{-1} K^{-1}] is the thermal conductivity of the fluid.
The heat transfer coefficient can be understood as

$$\alpha = -\lambda_\infty \cdot \frac{\frac{dT}{dz} \mid z = 0}{T_W - T_\infty} \tag{4.3}$$

where dT/dz is the temperature gradient in the z-direction.

4.2. Radiation

Bergman et al. [17] elucidated that while the transfer of energy by convection requires the presence of fluid to move through, the energy in the form of radiation is transported in a vacuum by electromagnetic waves. All objects emit radiation in accordance with their surface temperature. It can be posited that gases are transparent to radiation. A blackbody emits the highest amount of radiation possible for a given temperature. The total radiation emitted per unit area by a blackbody $\dot{q_{black}}$ [W m^{-2}] and the Stefan-Boltzmann law is

$$\dot{q_{black}} = \dot{e} = \sigma T^4 \tag{4.4}$$

where $\dot{e}$ [W m^{-2}] is the energy emitted per unit surface area of the black radiator and $\sigma = 5{,}67 \times 10^{-8}$ [W m^{-2} K^{-4}] is the Stefan-Boltzmann constant.
Radiation emitted by real surfaces, known as grey bodies, is lower than that emitted by a black body at the same temperature. Assuming two parallel surfaces with the emissivities ε_1 [-], ε_2 [-] and the temperatures T_1 [K], T_2 [K], the heat flux $\dot{q_{rad}}$ [W m^{-2}] is

$$\dot{q_{rad}} = \frac{1}{\frac{1}{\varepsilon_1} + \frac{1}{\varepsilon_2} - 1} \cdot \sigma \cdot (T_1^4 - T_2^4) \tag{4.5}$$

where $T_1 > T_2$.
The figure 4.3 shows a comparison between a blackbody and a real surface. While the

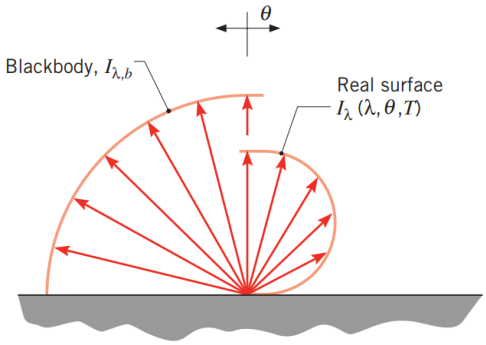

Figure 4.3: Blackbody and real surface emission, edited and adopted from [17]

blackbody emits with the intensity of wavelength λ_{wave} [μm] depending on the surface temperature, the emissivity of the real surface is additionally characterised by the zenith angle θ [rad].

4.3. Conduction

Conduction can be analysed using Fourier's law, which is applicable to different geometries. The heat flux $\dot{q_{cond}}$ [W m^{-2}] in a one-dimensional area is shown in figure 4.4 and defined as follows

$$\dot{q_{cond}} = -\lambda \cdot \frac{dT}{dz} \tag{4.6}$$

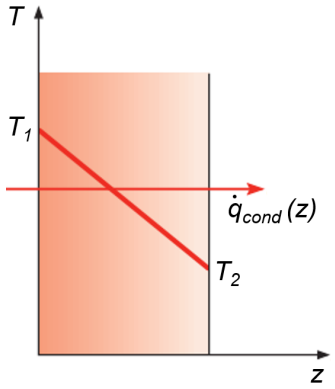

Figure 4.4: Conductive heat transfer in one dimension, edited and adopted from [17]

4.4. Flow in small channels

Given the relatively small gap ratio between the rotor and stator, the flow in the axial direction can be considered to be laminar. Thermal conductivity and convection are considered at the molecular level. Nusselt number in axial direction Nu_z [-] for an incompressible fluid is given by $Nu_z = 8{,}23$. [17]

4.4.1. Thermophysical properties of working fluid

Thermophysical properties exert a significant influence on the description of the heat transfer. In the context of forced convection, the thermal conductivity, dynamic viscosity, density and specific heat capacity are of significant importance [18].
It can be assumed that exhaust gases, including carbon dioxide, water vapour, nitrogen oxides and carbon monoxide, which operate at high temperatures within a narrow cavity, can be disregarded when considering their thermophysical properties. However, this assumption might lead to inaccuracies at lower local radii with laminar flow.

4.4.2. Dimensionless numbers

Prandtl number

The Prandtl number Pr [-] is a ratio of physical properties and is given by

$$Pr = \frac{\mu \cdot c_p}{\lambda} \tag{4.7}$$

The Prandtl number of gases is subject to a slight degree of variation in response to changes in temperature [18]. It is a commonly observed phenomenon that the Prandtl number for air within the rotor-stator system typically falls around 0,72.

Grashof number

The Grashof number Gr [-] shows how buoyancy forces compare to viscous forces within the velocity boundary layer. [17]

Reynolds number

As mentioned in the previous chapter, the Reynolds number is used to characterise the nature of the flow.
Harmand et al. [19] defined the Reynolds number in interdisc spacing Re_z [-] as follows

$$Re_z = G^2 \cdot Re_\phi \tag{4.8}$$

Nusselt number

The Nusselt number Nu [-] is a dimensionless heat transfer coefficient, which is given by

$$Nu = \frac{\alpha \cdot b}{\lambda_\infty} \tag{4.9}$$

For forced convection, the Nusselt number is a function of the Reynolds number and the Prandtl number:

$$Nu = f_1(Re, Pr) \tag{4.10}$$

For natural convection, the Nusselt number is a function of the Grashof number and the Prandtl number:

$$Nu = f_2(Gr, Pr) \tag{4.11}$$

Local Nusselt number

The local Nusselt number in a radial direction $Nu(r)$ [-] is a function of radial position. It can be defined by

$$Nu(r) = a \cdot Re_\phi(r)^b \tag{4.12}$$

where the coefficient a [-] is dependent on the flow regime, Prandtl number and the radial temperature distribution on the disc surface, while b [-] is dependent on the disc Reynolds number, respectively.
In their study, Harmand et al. [19] cite the local Nusselt number for air at $Pr = 0{,}72$ with laminar flow given over the entire disc as follows:

$$Nu_{lam} = 0{,}3286 \cdot Re_\phi(r)^{0{,}5} \tag{4.13}$$

Harmand et al. [19] proposed the local Nusselt number for turbulent flow (regime III), where the heat transfer depens on the gap ratio and the rotational speed:

$$Nu_{III}(r) = 0{,}01176 \cdot \left(\frac{r}{b}\right)^{\frac{7}{4}} \cdot G^{-\frac{1}{4}} \cdot Re_\phi^{\frac{3}{4}} \tag{4.14}$$

Couette Reynolds number

Couette Reynolds number $Re_{Couette}$ [-] is defined by the flow in the cavity:

$$Re_{Couette} = \frac{\Omega \cdot s \cdot b}{\nu} = Re_\phi \cdot G \tag{4.15}$$

5. Application of methodology to TCR16 turbocharger

This bachelor's thesis examines the water-cooled turbocharger TCR16, designed by PBS Turbo for use in locomotives and industrial applications.

Table 5.1: Geometric and thermophysical data

	Parameter	Dimension
Working fluid	Air	
	Density (ρ)	0,4 kg m^{-3}
	Inlet temperature (T_{Tin})	659,7 °C
	Kinematic viscosity (ν)	8×10^{-5} m^2 s^{-1}
	Outlet temperature (T_{Tout})	424 °C
	Prandtl number (Pr)	0,72
	Specific heat capacity (c_p)	1127 J/kg·K
	Thermal conductivity (λ_∞)	0,064 W/m·K
Turbine wheel	Inconel 713C	
	Angular velocity (Ω)	4712,4 rad/s
	Emissivity (ε_{rotor})	0,4
	Rotor speed (n)	45000 rpm
	Surface roughness (k_a)	$0{,}0163 \times 10^{-3}$ m
	Thermal conductivity (λ_{rotor})	8 W/m·K
Bearing casing		
	Emissivity (ε_{stator})	0,5

Determination of the flow regime

Table 5.2: Calculated results for TCR16 geometry

Point	$G(r)$	$Re_\phi(r)$	Flow	Boundary layer	Regime
0	0,026	577 000	turbulent	merged	III
1	0,05	209 000	turbulent	merged	III
2	0,056	119 000	laminar	separated	II
3	0,058	62 000	laminar	separated	II
4	0,05	24 000	laminar	separated	II

The cross-sectional view of TCR16 with axial clearance between the turbine disc face and the bearing casing wall is illustrated in figure 5.1. Various points along the disc radius were studied in detail.

Equation 3.8 was used to calculate Reynolds number, taking into account rotational speed at various local radii. The kinematic viscosity undergoes minor fluctuations at these points due to elevated temperatures during operation. A constant value of $\nu = 8 \times 10^{-5}$ m^2 s^{-1} was selected for each point.

The results were evaluated using equations 3.15; 3.9 - 3.10 whether the flow is turbulent or

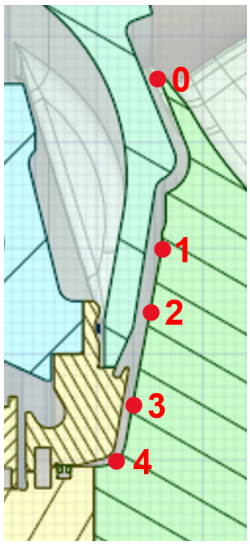

Figure 5.1: Points of interest, edited and adopted from the appendix A

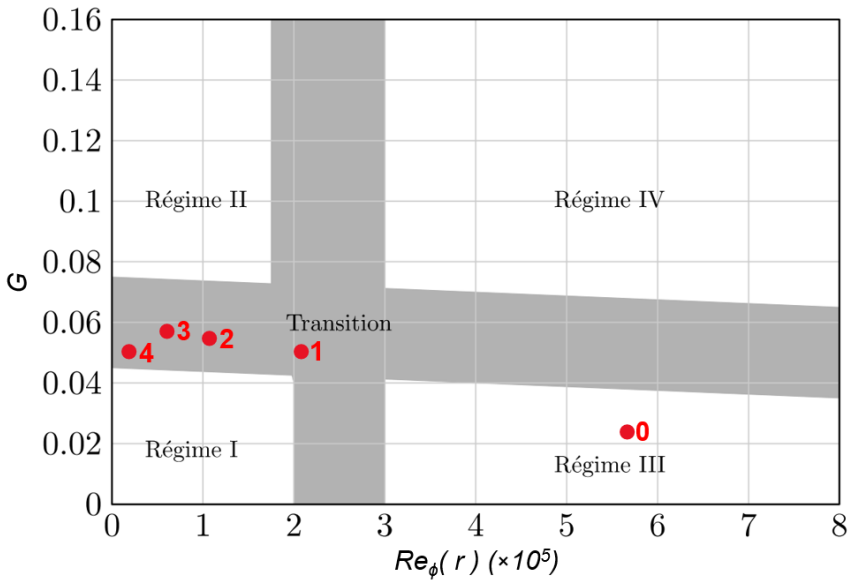

Figure 5.2: Locations in regimes according to calculated values, edited and adopted from [19]

laminar, respectively the boundary layer thickness. The calculated results are summarised in the table 5.2 and shown in figure 5.2.

Moment coefficient calculation

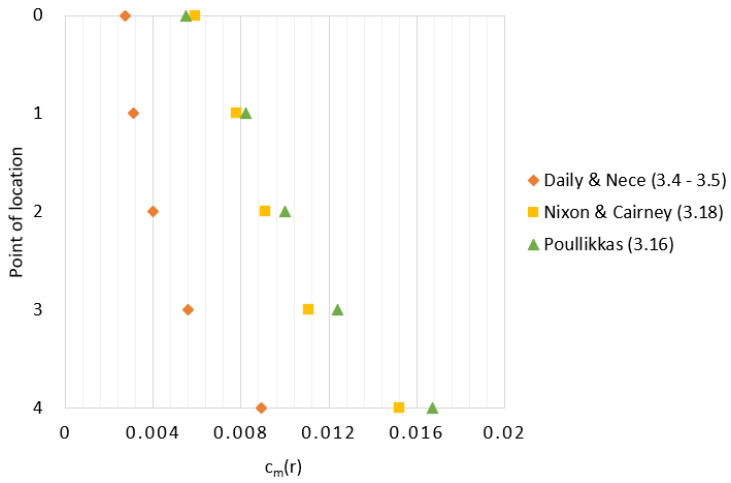

Figure 5.3: Moment coefficient at various points

The friction coefficient for each point was calculated using the equations 3.4 - 3.5; 3.16; 3.18 for smooth surface roughness with $k_a = 0{,}0163 \times 10^{-3}$ m and $t = 13 \times 10^{-3}$ m in 3.18. The moment coefficient is a single value that characterises the disc. Evaluations were conducted on each location point to assess potential variability depending on the radius. The results are shown in the graph 5.3.

Heat balance calculation

Boundary conditions

- Natural convection is negligible.
- The rotor disc is adiabatic.
- The stationary wall is isothermal, as it is constantly cooled by the oil and water systems.
- The mass flow within the cavity is negligible.

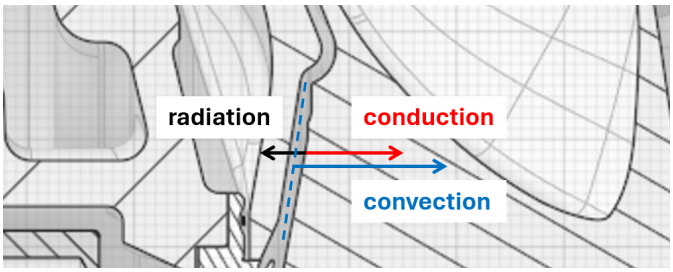

Figure 5.4: Heat transfer at the rotor side, edited and adopted from the appendix A

Figure 5.4 illustrates the distribution of heat transfer under the assumption that the fluid medium has a higher temperature than the turbine wheel. The thermal balance at the rear turbine disc can be defined as follows

$$\dot{q_{conv}} - \dot{q_{cond}} - \dot{q_{rad}} = 0 \tag{5.1}$$

where specific heat flux for convection is directed from the heated fluid medium to the rotor surface wall, while radiation acts from the turbine wheel to the bearing casing. Conduction is directed from the rear turbine side, traversing through the width of the impeller.
The figure 5.5 depicts the temperature distribution of the disc surface and fluid medium along the rotating wheels on the compressor and turbine sides, respectively. The temperature profile measured on the compressor side does not exhibit a precise correlation between the wall and fluid temperatures. However, the temperature decreases with the radius, with an average rate of change between the wall and fluid of approximately 20 °C. The analogy with the compressor wheel is employed to predict the fluid temperatures on the turbine side. At the inlet to the cavity, the fluid medium is predicted to have a temperature of 640 °C. This value is approximately 20 °C less than the temperature of the exhaust gases at the inlet, which is immediately after passing the nozzle ring. It is assumed that the maximum temperature difference is between the fluid and the wall at the outer disc radius. Predicted wall temperature is 580 °C. Based on the compressor analogy and the measured temperatures at the turbine disc surface, it can be estimated that the fluid temperature between the turbine wheel and bearing casing is approximately 20 °C higher along the entire radius. The estimated fluid temperatures for each location point are recorded in the table 5.3 and subsequently utilised for further calculations.

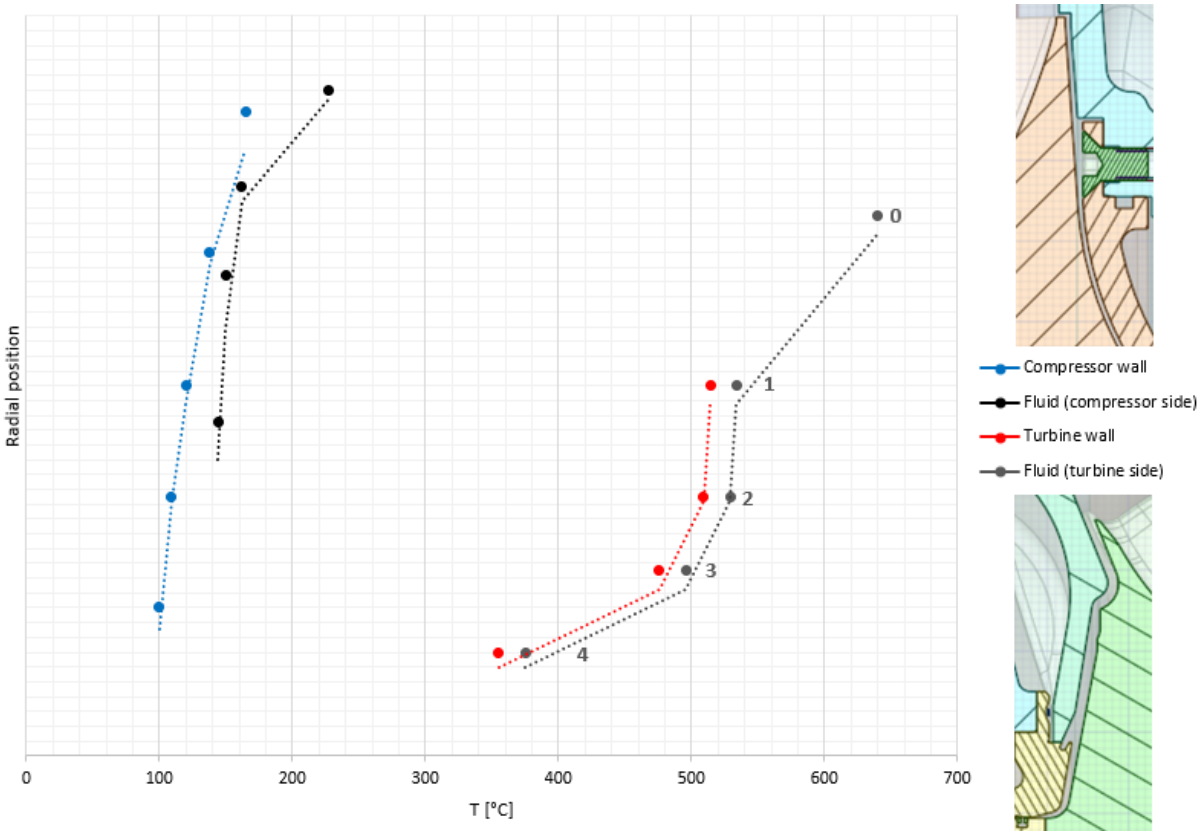

Figure 5.5: Measured and predicted temperature distribution on the compressor and turbine sides, edited and adopted from the appendix A

Table 5.3: Calculated, predicted and measured heat transfer data

Point	$c_m(r)$	$T_W(r)$ [°C]	$T_\infty(r)$ [°C]	$Nu(r)$	$\alpha(r)$ [W/m^2·K]
0	0,0055	580	640	613	396
1	0,0082	514,2	534	214	230
2	0,01	508,9	529	113	161
3	0,0124	475,9	496	82	161
4	0,0167	354,8	375	51	163

The local Nusselt number for turbulent and laminar cases was calculated using the equations 4.13 - 4.14.
A further calculation was performed to determine the local convective heat transfer coefficient.

$$\alpha(r) = \frac{Nu(r) \cdot \lambda_\infty}{r} \tag{5.2}$$

Table 5.4: Calculated results of the thermal balance

Segment	S_{10}	S_{21}	S_{32}	S_{43}
Heat flux ($\dot{q_{conv}}$)	23760 [W/m^2]	4554 [W/m^2]	3236 [W/m^2]	3236 [W/m^2]
Heat flow ($\dot{Q}$)	467 [W]	22 [W]	10 [W]	7 [W]

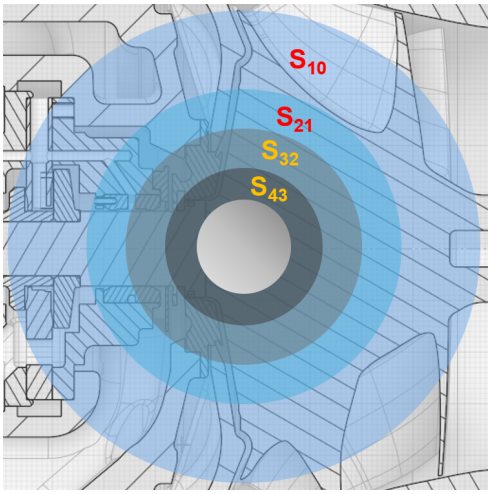

Figure 5.6: Surface segments, edited and adopted from the appendix A

The present study investigates the heat balance on the disc surface, which is divided into four segments, as illustrated in figure 5.6. The heat flux was calculated for each segment, taking into account the maximum heat transfer coefficient α_{max} [W/m^2·K] (points from 0 to 4):

$$\dot{q_{conv}} = \alpha_{max}(r) \cdot (T_W - T_\infty) \tag{5.3}$$

Heat flow for each segment is calculated as follows

$$\dot{Q} = \dot{q_{conv}} \cdot S_i = \dot{q_{conv}} \cdot \pi \cdot (r_{max}^2 - r_{min}^2) \tag{5.4}$$

where S_i [m^2] is the surface area of the segment with a circular ring shape. r_{max} [m] and r_{min} [m] are outer and inner radiuses of the circular ring.
The results are presented in the table 5.4, which demonstrates a clear decrease in heat flow with a decrease in radius. The results indicate that the total heat flow is 506 W. The result is notably low due to the relatively modest temperature gradient. This is due to the fact that the operating condition is considered to be one where the temperatures have reached their maximum after a certain period of time. In order to obtain accurate heat flux and heat flow values, it would be necessary to measure the flow temperature, similar to the approach used on the compressor side.
It is important to control the radiation on the outer radius of the disc when operating with high exhaust gases. In this study, the calculation of radiation is negligible due to the uncertainty surrounding the temperature of the bearing housing wall. Consequently, it can be deduced that conduction will be the highest at the outer radius.

Heat balance on the bearing housing

According to the VDI Heat Atlas [18], heat resistance is analogous to electrical resistance. Heat transmission on the bearing housing side can be considered in the form of one--dimensional heat transfer by convection and conduction through the walls. Figure 5.7 illustrates the conduction (areas A and C) and convection (areas B and D) processes in serial heat resistance. It is noteworthy that the area B represents the enclosed air cooling zone where an air vortex is observed. It is assumed that heat transfer in this area occurs

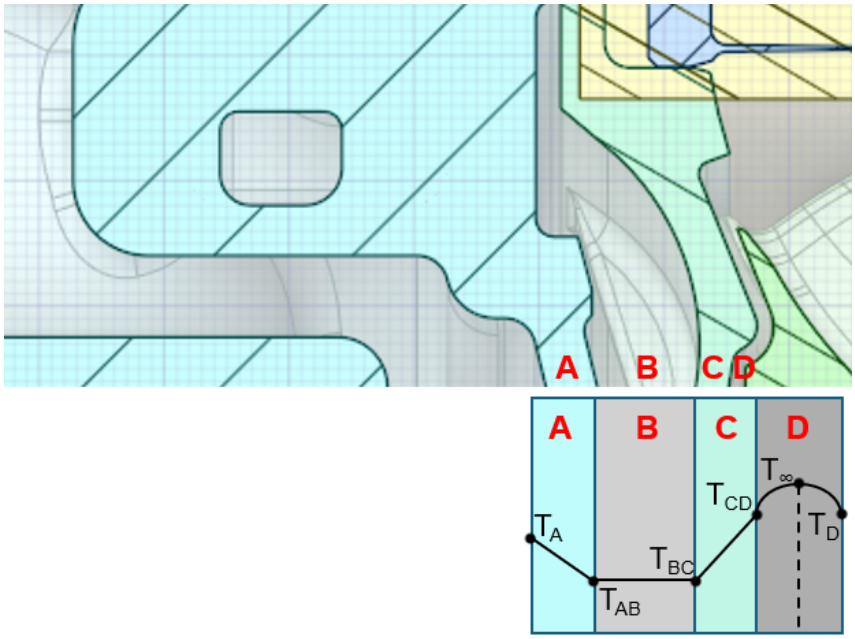

Figure 5.7: The series wall on the bearing housing side, edited and adopted from the appendix A

via conduction, with the fluid assumed to be a solid. The heat balance can be defined as a system of three equations

$$\frac{\lambda_A}{\delta_A} \cdot (T_A - T_{AB}) = \frac{\lambda_B}{\delta_B} \cdot (T_{AB} - T_{BC}) \tag{5.5}$$

$$\frac{\lambda_B}{\delta_B} \cdot (T_{AB} - T_{BC}) = \frac{\lambda_C}{\delta_C} \cdot (T_{BC} - T_{CD}) \tag{5.6}$$

$$\frac{\lambda_C}{\delta_C} \cdot (T_{CD} - T_{BC}) = \alpha \cdot (T_{CD} - T_\infty) + \sigma \cdot (T_D^4 - T_{CD}^4) \tag{5.7}$$

By solving the system of equations, it is possible to obtain the temperature T_{CD} at the stator surface. It is assumed that the wall temperature of the water passage is $T_A \approx 90\,°\mathrm{C}$.

5.1. Summary

The results of the friction moment analysis indicate that an increase in the radius of the disc will result in enhanced efficiency. Furthermore, it is expected that a reduction in the generation of heat energy will be observed.

6. Conclusion

The objective of the bachelor's thesis is to determine the heat balance at the point between the back of the turbine wheel and the bearing housing. The findings concerning the heat production and heat transfer in small channels of a rotor-stator system were derived from previously published works.

Theoretical and experimental studies have demonstrated that reliable calculations of friction losses are possible. The existing literature on the subject of flow problems identifies three main parameters that affect the flow structure in rotor-stator cavities: the Reynolds number of the rotor, the gap ratio, and the surface roughness. The findings of these studies have been applied to a real turbocharger. The friction coefficient has been evaluated at different radii to demonstrate prospective variability.

The primary focus of this study has been on the heat exchange between the fluid flow and the rotor wall, which occurs as a result of a temperature gradient. Heat energy is transferred through conduction, convection, and radiation. The convective heat flow has been evaluated on four segments in order to demonstrate prospective variability with changing disc radius. The evaluation of the heat flux through the turbine wheel has not been conducted due to the complex shape of the component. The calculation of radiation from the turbine wheel to the stator section has been omitted in this study, given the small temperature gradient considered in this study.

The model for the stator section is based on three interconnected systems of equations. The thermal resistance system employs the analogy of electrical resistance to determine the temperature on the bearing housing surface.

The following recommendations can be used in order of aerodynamic and thermal optimisation:

The smooth surface of the disc allows for a reduction in friction and heat production, which in turn leads to an improvement in the overall efficiency of the system. In order to reduce the friction coefficient, it is necessary to ensure that the flow is turbulent. The optimal ratio of disc radius to axial clearance is achieved when the velocity boundary layers are merged in an enclosed rotor-stator system.

To prevent the back of the turbine wheel from constantly operating at high temperatures, it is necessary to provide a more effective heat transfer on the stator side. This can be achieved by utilising a bearing housing material with high thermal conductivity.

References

[1] NGUYEN-SCHÄFER, H. *Rotordynamics of Automotive Turbochargers* [online]. Springer Tracts in Mechanical Engineering. Cham: Springer International Publishing, 2015. [cit. 2024-04-08]. ISBN 978-3-319-17643-7. Available from: doi: 10.1007/978-3-319-17644-4

[2] WATSON, N. and JANOTA, M.S. *Turbocharging the Internal Combustion Engine* [online]. Bloomsbury Publishing, 1982. [cit. 2024-03-24]. ISBN 9781349040247. Available from: doi: 10.1007/978-1-349-04024-7

[3] Turbocharger Bearing Systems. In: *Garrett Advancing Motion* [online]. [cit. 2024-04-19]. Available from: https://www.garrettmotion.com/de/knowledge-center--category/turbo-replacement/turbocharger-bearing-systems

[4] ZADOROZHNAYA, E.; HUDYAKOV, V. and SIBIRYAKOV, S. *Simulation of heat transfer in a turbocharger bearing housing* [online]. Tribology and Materials, 2022, 1(2), pp. 42-54. [cit. 2024-04-08]. ISSN 28129717. Available from: doi: 10.46793/tribomat.2022.007

[5] How Are Most Turbochargers Lubricated? In: *Goldfarb and Associates* [online]. Scott Goldfarb, 2023. [cit. 2024-04-08]. Available from: https://goldfarbinc.com/blogs/news/how-are-most-turbochargers-lubricated

[6] Water Cooling For Your Turbo. In: *Garrett Advancing Motion* [online]. [cit. 2024-04-19]. Available from: https://www.garrettmotion.com/racing-and-performance/choosing-a-turbocharger/water-cooling-for-your-turbo

[7] SULTANIAN, B. *Internal Flow around Rotors and Stators* [online]. Gas Turbines. Cambridge University Press, 2018, pp. 182-236. [cit. 2024-03-24]. ISBN 9781316755686. Available from: doi: 10.1017/9781316755686.005

[8] CHILDS, PETER R.N. *Rotating Flow.* Oxford: Elsevier, 2011. ISBN 978-0-12-382098-3.

[9] DAILY, J.W. and NECE, R.E. *Chamber Dimension Effects on Induced Flow and Frictional Resistance of Enclosed Rotating Disks* [online]. Journal of Basic Engineering, 1960, 82(1), pp. 217-230. [cit. 2024-03-25]. ISSN 0021-9223. Available from: doi: 10.1115/1.3662532

[10] PONCET, S. and SCHIESTEL, R. *Numerical modeling of heat transfer and fluid flow in rotor–stator cavities with throughflow* [online]. International Journal of Heat and Mass Transfer, 2007, 50(7-8), pp. 1528-1544. [cit. 2024-04-06]. ISSN 00179310. Available from: doi: 10.1016/j.ijheatmasstransfer.2006.08.028

[11] BERETTA, G.P. and MALFA, E. *Flow and heat transfer in cavities between rotor and stator disks* [online]. International Journal of Heat and Mass Transfer, 2003, 46(15), pp. 2715-2726. [cit. 2024-04-01]. ISSN 00179310. Available from: doi: 10.1016/S0017-9310(03)00065-6

[12] GOULBURN, J.R. and WILSON, J.H. *High speed disk friction losses in a gaseous medium* [online]. International Journal of Mechanical Sciences, 1975, 17(6), pp. 379-385. [cit. 2024-03-25]. ISSN 00207403. Available from: doi: 10.1016/0020-7403(75)90032-6

[13] POULLIKKAS, A. *Surface Roughness Effects on Induced Flow and Frictional Resistance of Enclosed Rotating Disks* [online]. Journal of Fluids Engineering, 1995, 117(3), pp. 526-528. [cit. 2024-03-25]. ISSN 0098-2202. Available from: doi: 10.1115/1.2817294

[14] NEMDILI, A. and HELLMANN, D.H. *Development of an Empirical Equation to Predict the Disc Friction Loss of a Centrifugal Pump* [online]. The 6th International Conference on Hydraulic Machinery and Hydrodynamics Timisoara, 2004, pp. 235–240. [cit. 2024-04-19]. Available from: https://api.semanticscholar.org/CorpusID:201801832

[15] Turbine Blade Optimization including Scallops for a Turbocharger. In: *CAESES* [online]. [cit. 2024-05-19]. Available from: https://www.caeses.com/industries/case-studies/turbine-blade-optimization-including-scallops-for-a-turbocharger

[16] HE, P.; SUN, Z.; ZHANG, H.; CHEN, H. and TAN, C. *Investigation of clearance flows in deeply scalloped radial turbines* [online]. Proceedings of the Institution of Mechanical Engineers, Part A: Journal of Power and Energy, 2012, 226(8), pp. 951-962. [cit. 2024-04-24]. ISSN 0957-6509. Available from: doi: 10.1177/0957650912460361

[17] BERGMAN, T.L.; DEWITT, D.P.; INCROPERA, F.P. and LAVINE, A.S. *Fundamentals of heat and mass transfer.* 7th ed. New York: John Wiley, 2011. ISBN 978-0470-50197-9.

[18] *VDI Heat Atlas.* Second Edition. Berlin: Springer, 2010. ISBN 978-3-540-77876-9.

[19] HARMAND, S.; PELLÉ, J.; PONCET, S. and SHEVCHUK, I.V. *Review of fluid flow and convective heat transfer within rotating disk cavities with impinging jet* [online]. International journal of thermal sciences, 2013, 67, pp. 1-30. [cit. 2024-05-11]. ISSN 1290-0729. Available from: doi: 10.1016/j.ijthermalsci.2012.11.009

List of abbreviations and symbols

$black$		Blackbody
lam		Laminar flow
$cond$		Conduction
$conv$		Convection
rad		Radiation
a	[-]	Coefficient of local Nusselt number
b	[-]	Coefficient of local Nusselt number
b	[m]	Outer disc radius
c_m	[-]	Moment coefficient
c_p	[J kg^{-1} K^{-1}]	Specific heat capacity at constant pressure
c_ω	[-]	Flow rate coefficient
$\dot{e}$	[W m^{-2}]	Energy emitted by blackbody
G	[-]	Gap ratio
Gr	[-]	Grashof number
h_i	[J kg^{-1}]	Specific enthalpy
k_a	[m]	Surface roughness parameter of the disc
$k_{a,crit}$	[m]	Critical value for surface roughness
$\dot{m}$	[kg s^{-1}]	Mass flow rate in the cavity
$\dot{m}_T$	[kg s^{-1}]	Mass flow rate in turbine stage
n	[rpm]	Rotational speed
Nu	[-]	Nusselt number
Nu_z	[-]	Nusselt number in the axial direction
Nu_{III}	[-]	Nusselt number for regime III
p_1	[Pa]	Pressure in the turbine inlet casing
p_5	[Pa]	Pressure in the turbine outlet casing
P_{DF}	[W]	Disc friction loss, mechanical power dissipation
P_T	[W]	The effective turbine output power
Pr	[-]	Prandtl number
$\dot{q}$	[W m^{-2}]	Heat flux
$\dot{Q}$	[W]	Heat flow
r	[m]	Local disc radius
Re_z	[-]	Reynolds number in the axial direction
$Re_{Couette}$	[-]	Couette Reynolds number

Re_ϕ	[-]	Circumferential Reynolds number
s	[m]	Axial gap width
S_i	[m^2]	Surface area of a segment i
t	[m]	Radial gap width
T_i	[K]	Thermodynamic temperature of a component i
T_q	[N m]	Moment, torque
T_W	[K]	Temperature at the disc surface
T_∞	[K]	Thermodynamic fluid temperature
T_1	[K]	Temperature in the inlet casing
u_r	[m s^{-1}]	Velocity component in the radial direction
u_z	[m s^{-1}]	Velocity component in the axial direction
u_ϕ	[m s^{-1}]	Velocity component in the tangential direction
U_i	[m s^{-1}]	Rotor tip speed
V_i	[m s^{-1}]	Absolute fluid velocity
W_i	[m s^{-1}]	Relative fluid velocity
$\dot{W}$	[W]	Total energy output in turbine stage
z	[m]	Axial coordinate
α	[W m^{-2} K^{-1}]	Heat transfer coefficient
δ	[m]	Boundary layer thickness
δ_i	[m]	Wall thickness
δ_T	[m]	Thermal boundary layer thickness
ε_i	[-]	Emissivity of a component i
η_T	[-]	Thermodynamic efficiency in turbine stage
θ	[rad]	Zenith angle
κ	[-]	Isentropic exponent of the air
λ_i	[W m^{-1} K^{-1}]	Thermal conductivity
λ_{wave}	[μm]	Wavelength
λ_∞	[W m^{-1} K^{-1}]	Thermal conductivity of the fluid
μ	[Pa s]	Dynamic viscosity
ν	[m^2 s^{-1}]	Kinematic viscosity
ρ	[kg m^{-3}]	Fluid density
σ	[W m^{-2} K^{-4}]	Stefan-Boltzmann constant
Ω	[rad s^{-1}]	Angular velocity of the disc

Appendix A

Temperatures TCR16.